Structural and Electronic Rearrangements upon the Oxidation of Binuclear (Ru_2) and Trinuclear ($MoRu_2$) Complexes with Bridging *o*-Phenylenediamido Ligands†

Adela Anillo,‡ M. Rosario Díaz,§ Santiago García-Granda,§ Ricardo Obeso-Rosete,*,‡ Agustín Galindo,*,|| Andrea Ienco,⊥ and Carlo Mealli*,⊥

Departamento de Química Orgánica e Inorgánica, Instituto Universitario de Química Organometálica "Enrique Moles", Facultad de Química, Universidad de Oviedo, Julián Clavería s/n 33071 Oviedo, Spain, Departamento de Química Física y Analítica, Facultad de Química, Universidad de Oviedo, Julián Clavería s/n 33071 Oviedo, Spain, Departamento de Química Inorgánica, Universidad de Sevilla, Apartado 553, 41071 Sevilla, Spain, and ICCOM, CNR, Via Madonna del Piano, 50019 Sesto Fiorentino, Firenze, Italy

Received October 9, 2003

The redox capabilities of some binuclear and trinuclear ruthenium complexes with bridging *o*-phenylendiamido ligands, $C_6H_4(NH)_2$-*o*, have been investigated. The known species $[Ru_2\{\mu\text{-}C_6H_4(NH)_2\text{-}o\}(\mu\text{-dppm})(CO)_2(PPh_3)_2]$ (**1**) and $[Ru_2Mo\{\mu\text{-}C_6H_4(NH)_2\text{-}o\}_2(CO)_6(PPh_3)_2]$ (**5**), reacted with $[Fe(Cp)_2](PF_6)$, yield the salts $[Ru_2\{\mu\text{-}C_6H_4(NH)_2\text{-}o\}(\mu\text{-dppm})(CO)_2(PPh_3)_2](PF_6)_2$ (**2**) and $[Ru_2Mo\{\mu\text{-}C_6H_4(NH)_2\text{-}o\}_2(CO)_6(PPh_3)_2](PF_6)_2\cdot CH_2Cl_2$ (**6**), respectively (dppm = $Ph_2PCH_2PPh_2$). Binuclear compounds analogous to **2** were obtained with pairs of PPh_3 or CO ligands in place of the diphosphine dppm. The redox properties of the compounds have been explored also with electrochemical methods. The structural determinations of **2** and **6** show, as an evident consequence of the oxidation, the bending of the originally upright $C_6H_4(NH)_2$-*o* bridge toward one metal that is eventually η^4-coordinated by the ligand. In the trinuclear species **6**, such a bending is limited to only one bridge and is directed toward the central molybdenum atom. Another structural consequence, attributable to electronic effects, is the reciprocal reorientation of two terminal L_3M fragments with modes that are different in **2** and **6**, respectively. These aspects have been highlighted through a theoretical analysis with DFT calculations and an extension of the perturbation theory arguments already introduced for the precursors **1** and **5**. There is evidence that, in each case, the oxidation affects mainly the bridging chelate $C_6H_4(NH)_2$-*o* that transforms from diamido to diimino in character. The activated back-donation from the η^4-coordinated metal into the diimino ligand causes also an evident weakening of the metal−metal bond. Complex **6** represents the first well-characterized case where one *o*-phenylenediamido and one *o*-diiminobenzene coexist as ligands.

Introduction

o-Phenylenediamido, $[C_6H_4(NH)_2\text{-}o]^{2-}$, a ligand that is commonly encountered in transition metal chemistry, represents a classic example of *noninnocent* behavior.[1] In fact, besides the dianionic form, also the monoanionic (*o*-benzosemiquinonediimino[2]) and neutral (*o*-diimino-benzene[3]) ones are observed in the coordination to a single metal center (Scheme 1).

Scheme 1

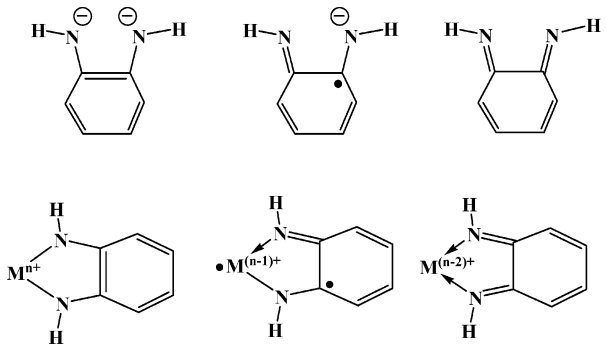

The bonding capabilities of *o*-phenylenediamido have attracted the attention of chemists since the initial

† Dedicated to Professor José Vicente on the occasion of his 60th birthday.

‡ Instituto Universitario de Química Organometálica "Enrique Moles", Universidad de Oviedo.

§ Departamento de Química Física y Analítica, Universidad de Oviedo.

|| Universidad de Sevilla.

⊥ ICCOM, CNR.

(1) See for example: Ward, M. D.; McCleverty, J. A. *J. Chem. Soc., Dalton Trans.* **2002**, 275, and references therein.

(2) Selected recent references concerning *o*-semiquinonato type ligands are: (a) Patra, S.; Sarkar, B.; Mobin, S. M.; Kaim, W.; Lahiri, G. K. *Inorg. Chem.* **2003**, *42*, 6469. (b) Ray, K.; Weyhermüller, T.; Goossens, A.; Crajé, M. W. J.; Wieghardt, K. *Inorg. Chem.* **2003**, *42*, 4082. (c) Chun, H.; Chaudhuri, P.; Weyhermüller, T.; Wieghardt, K. *Inorg. Chem.* **2002**, *41*, 790. (d) Chaudhuri, P.; Verani, C. V.; Bill, E.; Bothe, E.; Weyhermüller, T.; Wieghardt, K. *J. Am. Chem. Soc.* **2001**, *123*, 2213.

(3) The chemistry of diimino ligands has been reviewed: (a) van Koten, G.; Vrieze, K. *Adv. Organomet. Chem.* **1982**, *21*, 151. (b) Vrieze, K. *J. Organomet. Chem.* **1986**, *300*, 307.

10.1021/om034223k CCC: $27.50
Publication on Web 01/08/2004

synthesis of $[Ni(C_6H_4(NH)_2\text{-}o)_2]$ in 1926.[4] The interest has grown in recent years on account of the often unusual spectroscopic properties, the rich redox behavior, and other remarkable properties.[5,6] Also from the theoretical viewpoint, the metal−ligand orbital mixing, the electronic distribution, and the nature of the ground state have been the subject of several studies.[7,8] Being continuously intrigued by the behavior of the *o*-phenylenediamido ligand, we have recently carried out DFT calculations for complexes formed by the chelate with metals of groups 8 and 6. Thus, we have highlighted the electronic factors that underlie the *o*-phenylenediamido/*o*-diiminobenzene dichotomy in six- and five-coordinated mononuclear complexes of ruthenium.[9] Conversely, the diamido formulation seems to be a constant for the pseudo-octahedral complexes of Cr, Mo, and W, despite the wide range of metal oxidation states (from 0 to VI).[10]

The majority of the experimental and theoretical studies in this area are devoted to mononuclear compounds. In fact, there are only a few experimental examples of binuclear and polynuclear compounds in which the ligand $C_6H_4(NH)_2$-*o* acts as a bridge between two metal centers. Among the latter, the binuclear and trinuclear species, $[Ru_2\{\mu\text{-}C_6H_4(NH)_2\text{-}o\}(\mu\text{-dppm})(CO)_2(PPh_3)_2]$ (**1**)[11] and $[Ru_2Mo\{\mu\text{-}C_6H_4(NH)_2\text{-}o\}_2(CO)_6(PPh_3)_2]$ (**5**),[12] respectively, were characterized by some of us (see Scheme 2). While compound **1** has congeners of general formula $[Ru_2\{\mu\text{-}C_6H_4(NH)_2\text{-}o\}L_6]$ (L = CO or phosphine donor),[13] **5** remains unique in the literature. Also in other previous publications, we analyzed the electronic structure of both **1** and **5** by using the EHMO method and perturbation theory arguments.[14,15]

In the course of still ongoing experimental studies of these polynuclear ruthenium compounds, we decided to explore the redox properties of **1**, **5**, and some of their congeners. Here, we report the synthesis and the structural characterization of the dications $[Ru_2\{\mu\text{-}C_6H_4(NH)_2\text{-}o\}(\mu\text{-dppm})(CO)_2(PPh_3)_2]^{2+}$ and $[Ru_2Mo\{\mu\text{-}C_6H_4(NH)_2\text{-}o\}_2(CO)_6(PPh_3)_2]^{2+}$ obtained via a two-electron chemical oxidation of the uncharged precursors. In any case, there is a stereochemical rearrangement that raises interesting questions about the electronic redistribution within the primary frameworks. In particular, it must be established whether the electron pair is removed from the *o*-phenylenediamido ligand or the two bridged metal atoms that change oxidation state accordingly. In the attempt of finding a convincing answer to the question and also in order to understand better the role of $C_6H_4(NH)_2$-*o* as bridging ligand in a polynuclear system, we have performed detailed DFT calculations on both precursors and derivatives of the binuclear and trinuclear complexes.

Scheme 2

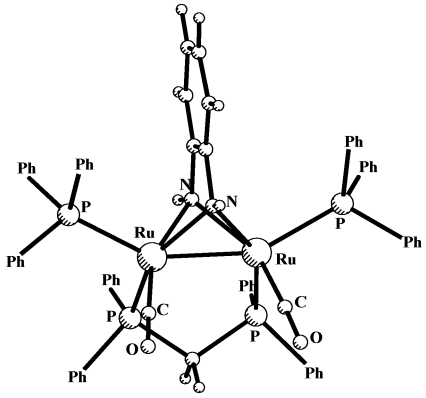

1

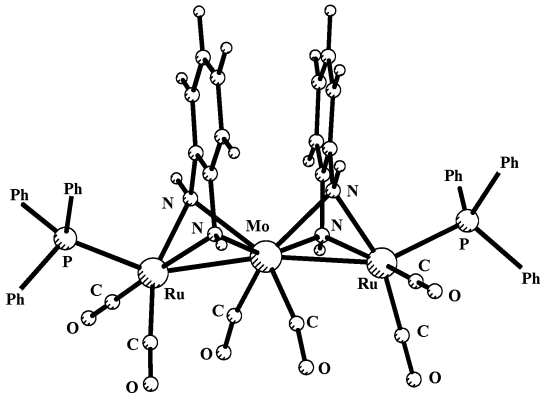

5

Experimental Section

General Procedures. All synthetic operations, NMR, and CV measurements were carried out under a dry nitrogen atmosphere. Solvents were freshly distilled using standard methods. IR spectra were recorded in Nujol mulls (KBr disks) or CH_2Cl_2 solutions (CaF_2 disks) on a Perkin-Elmer 1720-XFT spectrophotometer. NMR spectra (CD_2Cl_2 solutions) were recorded on a Bruker AC-300 spectrometer. Chemical shift data were referenced to tetramethylsilane (^1H) and to 85% external H_3PO_4 ($^{31}P\{^1H\}$). Cyclic voltammetric measurements were carried out with an Amel Electrochemolab instrument, using a three-electrode cell. The working and auxiliary electrodes were of platinum, and the reference one was an aqueous saturated calomel solution, separated from the solution of the complex by a porous frit and a KCl-saturated agar bridge. Measurements were carried out in CH_2Cl_2 solutions (ca. 0.5×10^{-3} M) with $(NBu^n_4)PF_6$ as supporting electrolite (0.1 M), at 50 mV s^{-1} scan rate. Conductivity data were obtained from a Crison micro CM 2201 conductimeter. Microanalytical data (C, H, and N) were obtained from a Perkin-

(4) Feigl, F.; Fürth, M. *Monatsh. Chem.* **1927**, *48*, 445.
(5) Jüstel, T.; Bendix, J.; Metzler-Nolte, N.; Weyhermüller, T.; Nuber, B.; Wieghardt, K. *Inorg. Chem.* **1998**, *37*, 35.
(6) (a) Das, C.; Kamar, K. K.; Ghosh, A. K.; Majundar, P.; Hung, C.-H.; Goswami, S. *New J. Chem.* **2002**, *26*, 1409. (b) Saha, A.; Das, C.; Mitra, K. N.; Peng, S.-M.; Lee, G. H.; Goswami, S. *Polyhedron* **2002**, *21*, 97. (c) Ghosh, A. K.; Peng, S.-M.; Paul, R. L.; Ward, M. D.; Goswami, S. *J. Chem. Soc., Dalton Trans.* **2001**, 336. (d) Mitra, K. N.; Choudhury, S.; Castiñeiras, A.; Goswami, S. *J. Chem. Soc., Dalton Trans.* **1998**, 2901.
(7) (a) Gorelsky, S. I.; Lever, A. B. P.; Ebadi, M. *Coord. Chem. Rev.* **2002**, *230*, 97. (b) Gorelsky, S. I.; Lever, A. B. P. *J. Organomet. Chem.* **2001**, *635*, 187. (c) Lever, A. B. P.; Gorelsky, S. I. *Coord. Chem. Rev.* **2000**, *208*, 153.
(8) Bachler, V.; Olbrich, G.; Neese, F.; Wieghardt, K. *Inorg. Chem.* **2002**, *41*, 4179.
(9) Anillo, A.; Garcia-Granda, S.; Obeso-Rosete, R.; Galindo, A.; Ienco, A.; Mealli, C. *Inorg. Chim. Acta* **2003**, *350*, 557.
(10) Galindo, A.; Ienco, A.; Mealli C. *Comments Inorg. Chem.* **2002**, *23*, 401.
(11) Anillo, A.; Obeso-Rosete, R.; Pellinghelli, M. A.; Tiripicchio, A. *J. Chem. Soc., Dalton Trans.* **1991**, 2019.
(12) Anillo, A.; Garcia-Granda, S.; Obeso-Rosete, R.; Rubio-Gonzalez J. M. *J. Chem. Soc., Dalton Trans.* **1993**, 3287.
(13) Garcia-Granda, S.; Obeso-Rosete, R.; Rubio J. M.; Anillo, A. *Acta Crystallogr. Sect. C* **1990**, *46*, 2043.
(14) Mealli, C.; Ienco, A.; Anillo, A.; Garcia-Granda, S.; Obeso-Rosete, R. *Inorg. Chem.* **1997**, *36*, 3724.
(15) Mealli, C.; Ienco, A.; Anillo, A.; Garcia-Granda, S.; Obeso-Rosete, R. *J. Chem. Soc., Dalton Trans.* **1997**, 1441.

Elmer 240-B elemental analyzer. $[Fe(Cp)_2]PF_6$ was purchased from commercial sources and was used without further purification. Complexes **1**, **3**, and **5** were prepared according to published methods.[11,12]

Syntheses of $[Ru_2\{\mu\text{-}C_6H_4(NH)_2\text{-}o\}(\mu\text{-dppm})(CO)_2(PPh_3)_2](PF_6)_2$ (2). The complex $[Ru_2\{\mu\text{-}C_6H_4(NH)_2\text{-}o\}(\mu\text{-dppm})(CO)_2(PPh_3)_2]\cdot C_6H_5CH_3$ (**1**) (0.100 g, 0.073 mmol) and $[Fe(Cp)_2]PF_6$ (0.048 g, 0.146 mmol) were stirred in CH_2Cl_2 (10 mL) for 15 min, at room temperature. From the mixture the solvent was removed by evaporation under vacuum. The residue was washed with hexane (4 × 5 mL), and the resulting yellow-brown solid was dried under vacuum (ca. 93% yield). Crystals suitable for X-ray were grown from a CH_2Cl_2−hexane solution. IR (Nujol mull, cm^{-1}): 3315 m, 3301 m, 1999 vs, 1981 vs, 1952 w, 1936 w (3309 w, 2004 vs, 1992 s-sh, in CH_2Cl_2 solution) and 843 vs,br. $^{31}P\{^1H\}$ NMR (δ, ppm): 72.15 t, 44.38 d, 21.03 t, 14.41 q, all coupling constants approximately 22 Hz. Conductivity (10^{-3} M solution in CH_3NO_2 at room temperature): 140 S cm^2 mol^{-1}. Anal. Calcd for $C_{69}H_{58}F_{12}N_2P_6O_2Ru_2$ (1563.17): C, 53.02; H, 3.74; N, 1.79. Found: C, 52.69; H, 3.82; N, 1.75.

Oxidation of $[Ru_2\{\mu\text{-}C_6H_4(NH)_2\text{-}o\}(CO)_4(PPh_3)_2]$: Attempted Synthesis of $[Ru_2\{\mu\text{-}C_6H_4(NH)_2\text{-}o\}(CO)_4(PPh_3)_2](PF_6)_2$ (4). The complex $[Ru_2\{\mu\text{-}C_6H_4(NH)_2\text{-}o\}(CO)_4(PPh_3)_2]\cdot C_6H_5CH_3$ (**3**) (0.100 g, 0.099 mmol) and $[Fe(Cp)_2]PF_6$ (0.066 g, 0.198 mmol) were stirred in CH_2Cl_2 (8 mL) for 10 min. The resulting mixture was worked up as stated above to obtain a yellow solid in ca. 95% yield. IR (Nujol mull, cm^{-1}): 3307 s, 2094 vs, 2071 vs, 2051 vs, 2023 vs (3306 w, 2089 s, 2074 vs, 2044 m, 2025 s, in CH_2Cl_2 solution) and 838 vs,br. $^{31}P\{^1H\}$ NMR (δ, ppm): two species, 69.10 d (J_{PP} = 22.3 Hz), 64.56 s, 38.48 s and 32.81 d (J_{PP} = 22.3 Hz). Anal. Calcd for $C_{46}H_{36}F_{12}N_2P_4O_4Ru_2$ (1234.80): C, 44.74; H, 2.94; N, 2.27. Found: C, 44.42; H, 3.06; N, 2.25.

Oxidation of $[Ru_2\{\mu\text{-}C_6H_4(NH)_2\text{-}o\}(CO)_3(PPh_3)(dppe)]$: Attempted Synthesis of $[Ru_2\{\mu\text{-}C_6H_4(NH)_2\text{-}o\}(CO)_3(PPh_3)(dppe)](PF_6)_2$. The complex $[Ru_2\{\mu\text{-}C_6H_4(NH)_2\text{-}o\}(CO)_3(PPh_3)(dppe)]\cdot C_6H_5CH_3$ (0.093 g, 0.081 mmol) and $[Fe(Cp)_2]PF_6$ (0.054 g, 0.163 mmol) were dissolved in CH_2Cl_2 (10 mL) and stirred for 15 min. The resulting mixture was worked up as stated above to obtain a yellow solid in ca. 92% yield. IR (Nujol mull, cm^{-1}): 3322 m, 2067 vs, 2044 vw, 2019 vs, 1982 s (3311 w, 2068 vs, 2013 vs, 1986 m in CH_2Cl_2 solution) and 844 vs,br. $^{31}P\{^1H\}$ NMR (δ, ppm): 70.26 d (J_{PP} = 17.7 Hz), 65.98 d (J_{PP} = 17.7 Hz) and 48.96 s. Anal. Calcd for $C_{53}H_{45}F_{12}N_2P_5O_3Ru_2$ (1342.93): C, 47.40; H, 3.38; N, 2.09. Found: C, 47.71; H, 3.42; N, 2.03.

Syntheses of $[Ru_2Mo\{\mu\text{-}C_6H_4(NH)_2\text{-}o\}_2(CO)_6(PPh_3)_2](PF_6)_2\cdot CH_2Cl_2$ (6). The complex $[Ru_2Mo\{\mu\text{-}C_6H_4(NH)_2\text{-}o\}_2(CO)_6(PPh_3)_2]\cdot C_6H_5CH_3$ (**5**) (0.100 g, 0.077 mmol) and $[Fe(Cp)_2]PF_6$ (0.051 g, 0.154 mmol) were stirred in CH_2Cl_2 (10 mL) for 20 min. The resulting mixture was worked up as stated above to obtain a brown solid in ca. 90% yield. Crystals suitable for X-ray were grown from a CH_2Cl_2−hexane solution. IR (Nujol mull, cm^{-1}): 3361 w, 3338 w, 3305 m, 2066 vs, 2050 s, 2014 vs, 2000 s (3343 w, 3303 w, 2067 vs, 2048 m, 2015 s, 1997 w in CH_2Cl_2 solution) and 841 vs,br. ^1H NMR (δ, ppm): 6.15 m, 5.77 s,br (intensity ratio 2:1). $^{31}P\{^1H\}$ NMR (δ, ppm): 56.83 s. Anal. Calcd for $C_{69}H_{58}F_{12}N_2P_6O_2Ru_2$ (1577.82): C, 41.87; H, 2.81; N, 3.55. Found: C, 42.31; H, 2.82; N, 3.69.

Crystal Structure Determination of Complexes 2 and 6. X-ray data were initially collected for both complexes on a Nonius CAD-4 single-crystal diffractometer at 293 ± 2 K (molybdenum radiation, λ = 0.71073 Å). The crystalline samples of compound **2** were of poor quality but did not prevent the collection of a sufficient number of reflections for structure solution. Difficulties in the subsequent structural refinement prompted us to try a second data collection at 200 K in order to prevent possible crystal deterioration, but the improvement was negligible. In fact, the *R* factor did not decrease below 11% and thermal ellipsoids were ill defined for some carbon atoms. For this reason, only the gross features of the structure are outlined in the paper and all the usual details are omitted.

For compound **6**, the unit cell parameters were obtained from the least-squares fit of 25 reflections (with θ between 4° and 12°), and an empirical absorption correction was performed at a later stage of refinement by using XABS2.[16] Maximum and minimum correction factors were, respectively, 0.93 and 0.80. The structure was solved by the Patterson methods and phase expansion using DIRDIF.[17] The full-matrix least-squares refinements on F^2 were carried out with the package SHELXL97.[18] Anisotropic thermal parameters were introduced at a later stage of refinement for all non-hydrogen atoms. Also hydrogen atoms were introduced and refined by using a restricted riding model. The highest electronic residuals were observed, as spurious peaks, in the close proximity of the Ru2 and P4 atoms. Atomic scattering factors were taken from International Tables for X-ray Crystallography (1974). The crystallographic plots were made with EUCLID.[19] All calculations are made at the University of Oviedo on the Scientific Computer Centre and X-ray group DEC/AXP-computers. Crystal data and details of the data collection and refinement are given in Table 1.

Computational Details. The electronic structure and geometries of the model complexes were computed within the density functional theory at the B3LYP[20] level using the LANL2DZ[21] basis set for the ruthenium and molybdenum atoms. The basis set used for the remaining atoms was the 6-31+G(d,p). All the optimized geometries were characterized as local energy minima by diagonalization of the analytically computed Hessian (vibrational frequency calculations). The DFT calculations were performed using the Gaussian 98 suite of programs.[22] Molecular orbitals were visualized using the GaussView program.[23] Cartesian coordinates for the optimized molecules are available from the authors upon request. The FMO analyses were made with CACAO[24] using the coordinates of the optimized model complexes.

Results and Discussion

Binuclear Compounds. The synthesis and structural characterization of the complex $[Ru_2\{\mu\text{-}C_6H_4(NH)_2\text{-}o\}(\mu\text{-dppm})(CO)_2(PPh_3)_2]$ (**1**) was reported years ago.[11]

(16) Parkin, S.; Moezzi, B.; Hope H. *J. Appl. Crystallogr.* **1995**, *28*, 53.

(17) Beurskens, P. T.; Beurskens, G.; De Gelder, R.; Garcia-Granda, S.; Israel, R.; Gould R. O.; Smits, J. M. M. *The DIRDIF-99 program system*; Crystallography Laboratory, University of Nijmegen: The Netherlands, 1999.

(18) Sheldrick, G. M. *SHELXL-97*, Program for the Refinement of Crystal Structures; University of Göttingen: Göttingen, Germany, 1997.

(19) Spek, A. L. *The EUCLID package*. In *Computational Crystallography*; Sayre, D., Ed.; Clarendon Press: 1982; p 528.

(20) (a) Becke, A. D. *J. Chem. Phys.* **1993**, *98*, 5648. (b) Lee, C.; Yang, W.; Parr, R. G. *Phys. Rev. B* **1988**, *37*, 785.

(21) (a) Dunning, T. H., Jr.; Hay, P. J. *Modern Theoretical Chemistry*; Plenum: New York, 1976; p 1. (b) Hay, P. J.; Wadt, W. R. *J. Chem. Phys.* **1985**, *82*, 299.

(22) Frisch, M. J.; Trucks, G. W.; Schlegel, H. B.; Scuseria, G. E.; Robb, M. A.; Cheeseman, J. R.; Zakrzewski, V. G.; Montgomery, J. A., Jr.; Stratmann, R. E.; Burant, J. C.; Dapprich, S.; Millam, J. M.; Daniels, A. D.; Kudin, K. N.; Strain, M. C.; Farkas, O.; Tomasi, J.; Barone, V.; Cossi, M.; Cammi, R.; Mennucci, B.; Pomelli, C.; Adamo, C.; Clifford, S.; Ochterski, J.; Petersson, G. A.; Ayala, P. Y.; Cui, Q.; Morokuma, K.; Malick, D. K.; Rabuck, A. D.; Raghavachari, K.; Foresman, J. B.; Cioslowski, J.; Ortiz, J. V.; Baboul, A. G.; Stefanov, B. B.; Liu, G.; Liashenko, A.; Piskorz, P.; Komaromi, Y.; Gomperts, R.; Martin, R. L.; Fox, D. J.; Keith, T.; Al-Laham, M. A.; Peng, C. Y.; Nanayakkara, A.; González, C.; Challacombe, M.; Gill, P. M. W.; Johnson, B.; Chen, W.; Wong, M. W.; Andrés, J. L.; Head-Gordon, M.; Replogle, E. S.; Pople, J. A. *Gaussian 98*, Revision A.9; Gaussian Inc.: Pittsburgh, PA, 1998.

(23) *GaussView 2.08*, Gaussian, Inc.: Pittsburgh, PA, 1998.

(24) (a) Mealli, C.; Ienco, A.; Proserpio, D. M. *Book of Abstracts of the XXXIII ICCC*; Florence, 1998; p 510. (b) Mealli, C.; Proserpio, D. M. *J. Chem. Educ.* **1990**, *67*, 399.

Table 1. Crystal Data, Data Collection, and Refinement for 2 and 6

	2	6
	Crystal Data	
formula	$C_{69}H_{58}F_{12}N_2O_2P_6Ru_2$	$C_{55}H_{44}Cl_2F_{12}MoN_4O_6P_4Ru_2$
molecular wt	1563.13	1577.8
color and habit	brown, irregular block	brown, irregular block
cryst size, mm	0.13 × 0.10 × 0.10	0.23 × 0.20 × 0.07
symmetry, space group	monoclinic, $P2_1/n$	triclinic, $P\bar{1}$
a, Å	12.731(4)	9.848(6)
b, Å	21.554(14)	10.398(6)
c, Å	25.55(4)	29.353(13)
α, deg	90	88.40(4)
β, deg	95.55(4)	84.80(5)
γ, deg	90	88.77(8)
V, Å^3	6978(11)	2992(3)
Z	4	2
D_{calc}, g/cm^3	1.488	1.752
	Data Collection and Refinement[a]	
λ(Mo, Kα), Å	0.71073	
monochromator	graphite-crystal	
scan type	$\omega-2\theta$ scan	
limiting indices	$0 \le h \le 12$	$-12 \le h \le 12$
	$0 \le k \le 20$	$-12 \le k \le 12$
	$-24 \le l \le 24$	$0 \le l \le 12$
μ, mm^{-1}	0.647	0.991
θ, range deg	1.24, 20.06	0.7, 26.15
temp, K	200	293
no. of data collected	6922	11 967
no. of unique data	6533 ($R_{int} = 0.2802$)	11 726 ($R_{int} = 0.0288$)
no. of params/restraints	309/2	723/0
final R indices R_1[b]	0.1189	0.0727
$[I > 2\sigma(I)]$ wR_2[b]	0.2643	0.1865
R indices (all data) R_1[b]		0.0936
wR_2[c]		0.2143
S		1.062
largest diff peak and hole e Å^{-3}		2.03, −3.30

[a] Due to the poor structural quality of **2**, only some basic details are reported. [b] $R_1 = \sum||F_o| - |F_c||/\sum|F_o|$. [c] $wR_2 = (\sum(w(F_o^2 - F_c^2)^2)/\sum w(F_o^2)^2))^{1/2}$.

The structure, depicted in Scheme 2, features a direct Ru−Ru bond of 2.562(1) Å and a symmetrically oriented *o*-phenylenediamido bridge that rides upright the sawhorse formed by the RuL_3 units. The congener of formula $[Ru_2\{\mu\text{-}C_6H_4(NH)_2\text{-}o\}(CO)_4(PPh_3)_2]$ has also been reported.[13] According to a previous theoretical analysis for this class of compounds, the diamido dianion donates up to four electron pairs to the two d^7 metals, while similar bonding capabilities do not straightforwardly apply to catecholate ligands.[14] Also, the analogous enediamido ligands, with no arylic backbone, have not been observed to ride across two metal atoms.

The oxidation of **1** with $[Fe(Cp)_2]PF_6$ (molar ratio 1:2) in a CH_2Cl_2 solution afforded a yellow-brown solution. After solvent evaporation and hexane washing to eliminate $Fe(Cp)_2$, a solid of the same color was obtained in high yields. The conductivity of the oxidized species, measured in acetonitrile, is close to that expected for a 1:2 electrolyte. Moreover, a strong IR band at about 840 cm^{-1}, which is typical of PF_6^- counterions, permits us to formulate the species as $[Ru_2\{\mu\text{-}C_6H_4(NH)_2\text{-}o\}(\mu\text{-dppm})(CO)_2(PPh_3)_2](PF_6)_2$ (**2**). The reduction of **2** with Na/Hg gave again the complex **1** without any detectable side species. Consistently with the presence of two carbonyl ligands, the IR spectrum of **2** shows two bands with frequencies (1999 and 1981 cm^{-1}) that are somewhat higher than those in the precursor **1** (1909, 1877 cm^{-1}). Additional IR bands that correspond to the ν(NH) stretching of the $C_6H_4(NH)_2$-*o* ligand were observed at about 3300 cm^{-1}. In **1**, as well as in other ruthenium complexes where the chelate is closer to the *o*-phenylenediamido formulation,[12,13,25] the ν(NH) band occurs at IR frequencies that are higher by about 40−50 cm^{-1}. In general, a ν(NH) band at lower frequencies is diagnostic of a less negative charge at the ligand. In particular, when the lowering of the ν(NH) band follows the chemical oxidation, as in the present case, it may be inferred that the $C_6H_4(NH)_2$-*o* dianion has converted to a monoanionic or neutral form. The $^{31}P\{^1H\}$ NMR spectrum of complex **2** shows a typical AMNX pattern consisting of one doublet (44.38 ppm), two triplets (at 72.15 and 21.03 ppm), and one quartet (14.41 ppm). The latter are relatable to four nonequivalent P nuclei and can be tentatively assigned to the atoms P_1, P_4, P_2, and P_3, respectively (refer to Figure 1 for the atomic labeling). Thus, a nonsymmetric structure is suggested by the nonequivalence of the two triphenylphosphine ligands as well as of the two P atoms belonging to the dppm chelate. An X-ray structure determination of **2** has been attempted to confirm the latter point, but, as mentioned in the Experimental Section, the results are of unsatisfactory quality. Here, we point out only some essential features. The structure consists of two PF_6^- anions for any dimeric dication $[Ru_2\{\mu\text{-}C_6H_4(NH)_2\text{-}o\}(\mu\text{-dppm})(CO)_2(PPh_3)_2]^{2+}$. The stereochemistry of the latter is depicted in Figure 1, and it is evident that the $C_6H_4(NH)_2$-*o* ligand is bent toward one ruthenium atom (Ru1) that is tetrahapto coordinated by the sequential atoms N1, C11, C12, and N2. At the same time the ligand acts as a normal dihapto σ chelate toward the other metal atom (Ru2). The present σ/π coordination mode is unprecedented for the ligand $C_6H_4(NH)_2$-*o*, but it has been documented for other binuclear ruthenium complexes containing simpler diimino ligands without an arylic backbone.[26] Another structural effect of the oxidation is the staggered orientation assumed by the two terminal RuL_3 fragments. Notice for example in Figure

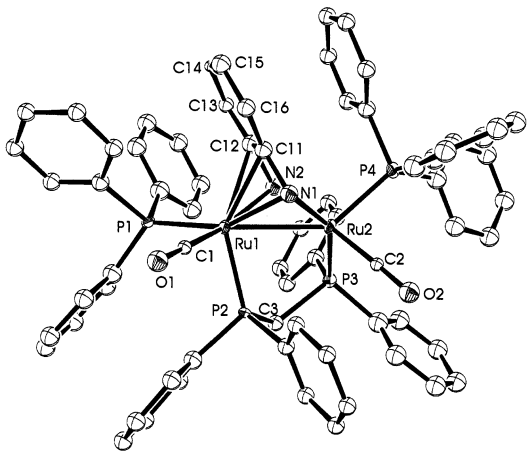

Figure 1. ORTEP drawing of the complex dication $[Ru_2\{\mu\text{-}C_6H_4(NH)_2\text{-}o\}(\mu\text{-dppm})(CO)_2(PPh_3)_2]^{2+}$ in compound **2**.

(25) Jüstel, T.; Bendix, J.; Metzler-Nolte, N.; Weyhermüller, T.; Nuber, B.; Wieghardt, K. *Inorg. Chem.* **1998**, *37*, 35.

(26) (a) Keijsper, J.; Polm, L.; van Koten, G.; Vrieze, K.; Abbell, G.; Stam, C. H. *Inorg. Chem.* **1984**, *23*, 2142. (b) Staal, L. H.; van Koten, G.; Vrieze, K.; Ploeger, F.; Stam, C. H. *Inorg. Chem.* **1981**, *20*, 1830.

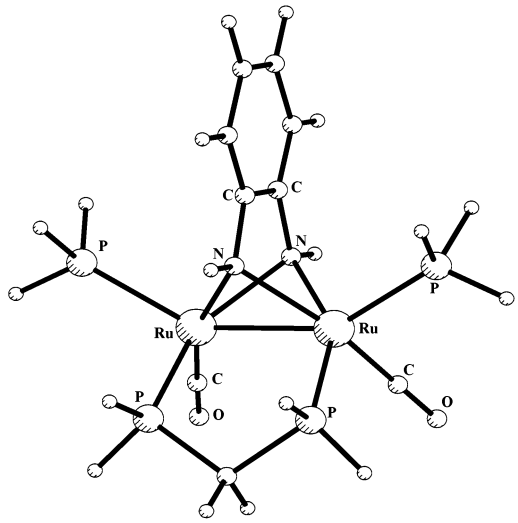

1a

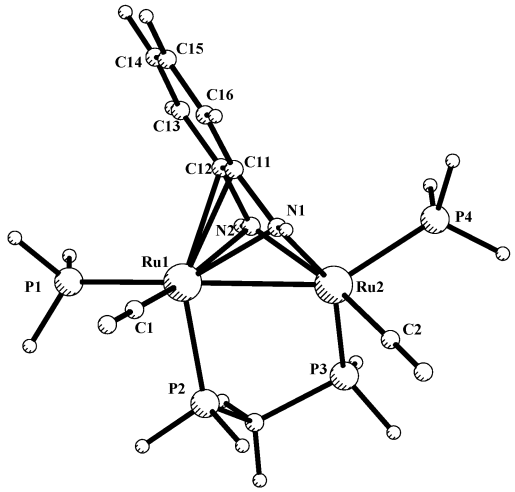

2a

Figure 2. Optimized structures of the models $[Ru_2\{\mu\text{-}C_6H_4(NH)_2\text{-}o\}(\mu\text{-}H_2PCH_2PH_2)(PH_3)_2(CO)_2]$ (**1a**) and $[Ru_2\{\mu\text{-}C_6H_4(NH)_2\text{-}o\}(\mu\text{-}H_2PCH_2PH_2)(PH_3)_2(CO)_2]^{2+}$ (**2a**).

1 how the dppm ligand now winds the Ru−Ru bond, the P2−Ru1−Ru2−P3 torsion angle being >40°. The Ru−Ru separation, the only geometric parameter to be focused on here, is definitely longer than that in the precursor **1** [2.844(5) vs 2.562(1) Å]. This aspect is fully confirmed by our DFT optimizations of the respective models (vide infra).

Discrimination between the diamido/diimino formulation of the $C_6H_4(NH)_2$-*o* or similar *noninnocent* ligand is often based on the relative C−C and C−N bond lengths.[27] As pointed out by Wieghardt et al.,[25,28] such a criterion requires X-ray data of high quality that are missing in this case. However, the comparison is meaningful between the model compounds $[Ru_2\{\mu\text{-}C_6H_4(NH)_2\text{-}o\}(\mu\text{-}H_2PCH_2PH_2)(PH_3)_2(CO)_2]$ (**1a**) and $[Ru_2\{\mu\text{-}C_6H_4(NH)_2\text{-}o\}(\mu\text{-}H_2PCH_2PH_2)(PH_3)_2(CO)_2]^{2+}$ (**2a**), which have been optimized at the same DFT level. The drawings of the latter, which carry H atoms in place of phenyl substituents at the phosphine groups, are presented in Figure 2. The species **1a** was optimized with C_s symmetry, and its structural parameters are presented in Table 2, together with those of complex **1**. The agreement is generally satisfactory with a good description of the metal−metal bond (2.583 vs 2.562(1) Å). The maximum deviation between any experimental and computed bond length is about +0.04 Å.

Table 2. Selected Structural Parameters of Calculated Model Complex 1a and the Corresponding Experimental Parameters

bond distances (Å) and angles (deg)	complex **1** (exptl)	complex **1a** (calcd)
Ru−Ru	2.562(1)	2.583
	2.289(2)	
$Ru-P_{bridge}$	2.277(2)	2.317
	2.372(2)	
Ru−P	2.374(3)	2.387
	1.832(8)	
Ru−CO	1.843(8)	1.872
	2.186(7)	
Ru−N	2.159(7)	2.177
	2.195(6)	2.221
	2.128(6)	
N−C	1.41(1)	1.415
	1.43(1)	1.417
C−C	1.41(1)	1.418
	1.36(1)	1.391
	1.39(1)	1.411
C−C (ring)	1.33(1)	1.391
	1.40(1)	1.411
	1.35(1)	1.389

Table 3. Computed Bond Distances (Å) of the Model 2a

Ru1−Ru2	2.826
Ru1−P1	2.384
Ru1−P2	2.356
Ru2−P3	2.365
Ru2−P4	2.326
Ru1−C1	1.913
Ru2−C2	1.911
Ru1−N1	2.241
Ru1−N2	2.236
Ru2−N1	2.076
Ru2−N2	2.144
Ru1−C11	2.382
Ru1−C12	2.413
N1−C11	1.395
N2−C12	1.394
C11−C12	1.443
C12−C13	1.418
C13−C14	1.382
C14−C15	1.422
C15−C16	1.379
C16−C11	1.421

The computed structural parameters of **2a** are collected in Table 3. The comparison of the Ru−Ru separation in both systems (2.583 Å in **1a** vs 2.826 Å in **2a**) confirms the weakening the metal−metal bond upon oxidation. The variations in the optimized geometry of the ligand $C_6H_4(NH)_2$-*o* can be discriminative of the redox process effects. Thus, the C−C and C−N distances within the metallacycle [1.418 and 1.416 (av) Å in **1a**] become elongated and shortened respectively in **2a** [1.443 and 1.3945 (av) Å]. Despite the small differences, the trend is suggestive of a diamido → diimino transformation. The point is further supported by the comparison of the computed C−C distances within the C_6 ring. While in **1a** they are all fairly close to 1.40 Å, in

(27) (a) Carugo, O.; Djinović, K.; Rizzi, M.; Castellani, C. B. *J. Chem. Soc., Dalton Trans.* **1991**, 1551. (b) Bhattacharya, S.; Gupta, P.; Basuli, F.; Pierpoint, C. G. *Inorg. Chem.* **2002**, *41*, 5810.

(28) Herebian, D.; Bothe, E.; Neese, F.; Weyhermüller, T.; Wieghardt, K. *J. Am. Chem. Soc.* **2003**, *125*, 9116.

Scheme 3

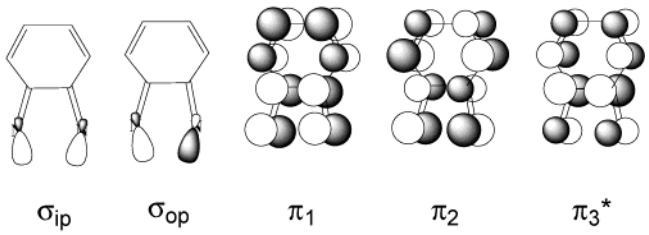

2a the C13−C14 and C15−C16 distances are about 1.38 Å and suggest localization of the C=C double bonds. According to the Mulliken charges, the ligand $C_6H_4(NH)_2$-*o* is computed to lose only one of the two electrons removed from **1a**, while the CO and phosphine ligands lose all together as many as 1.4 electrons. Although the metals appear 0.4 electron richer, the oxidation has clearly reduced the back-donating power toward the ligands in question. This is confirmed, in particular, by the CO frequencies since their computed values of 1928 and 1901 cm^{-1} for **1a** become 2043 and 2029 cm^{-1} for **2a**. This result is also consistent with the experimental trends. In conclusion, the oxidation determines mainly the diamido−diimino transformation, while the metals' back-donating power seems more affected than their actual oxidation state. The point can be further supported by an analysis of the MO electronic distribution.

We have previously presented a qualitative EHMO analysis to interpret the bonding capabilities of *o*-phenylenediamido and other similar ligands that ride upright a binuclear sawhorse.[14] In brief, we considered the diamido ligand as able to donate up to four electron pairs to the two metals. The MO combinations of $C_6H_4(NH)_2$-*o*, which act as donors toward the metals, are the first four depicted in Scheme 3. These include two filled σ lone pair combinations and two low lying π bonding levels (π_1 and π_2). Additionally the MO π_3*, which is at the same time C−C bonding and C−N antibonding, is critical, as it can be populated or depopulated. In the complexes of type **1**, π_3* and π_1 have the same b_1 symmetry, but the former is not a real donor on account of the poor overlap with the adapted metal orbitals. The HOMO of **1a**, as calculated at the DFT level (see Figure 3), is most similar to π_3* and is almost exclusively centered on the riding ligand. This confirms the diamido character of $C_6H_4(NH)_2$-*o* in the complex. The next filled MO (right side of Figure 3) is the bent metal−metal bonding combination that is expected for a d^7−d^7 dinuclear compound assembled from two local square pyramids.

The oxidation process occurring at the HOMO should in principle promote the transformation of the diamido into a diimino ligand. Still, four ligand combinations (two σ ones, plus π_1 and π_2) are available to saturate the d^7−d^7 sawhorse. However, on emptying π_3*, the HOMO−LUMO gap becomes too small and Jahn−Teller second-order effects are triggered. Structural rearrangements, such as the bending of $C_6H_4(NH)_2$-*o*, the relative reorientation of the two RuL_3 fragments, and the ∼0.3 Å elongation of the Ru−Ru bond, ensue. To understand better these effects, we have optimized, further simplified, and symmetrized the models of **1** and **2**. Thus, all of the phosphine donors were replaced with CO ligands; moreover, the ligand HN=CH−CH=NH (DAD) was

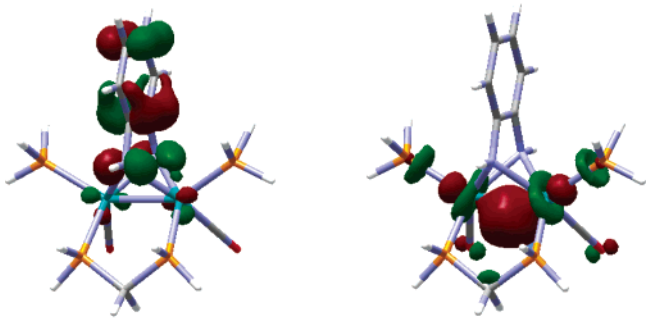

Figure 3. 3D isosurfaces corresponding to the HOMO and HOMO-1 of **1a**.

used in place of $C_6H_4(NH)_2$-*o*.[29] The optimized structures of $[Ru_2(DAD)(CO)_6]$ (**1b**) and $[Ru_2(DAD)(CO)_6]^{2+}$ (**2b**) are consistent with those of **1** and **2** and their closest models **1a** and **2a** (see Figure 4).

The complex dication $[Ru_2(DAD)(CO)_6]^{2+}$ has also been optimized as a transition state (**2TS**) in which the ligand DAD is bent toward the Ru2 metal, while the two terminal RuL_3 fragments are still eclipsing each other as in the precursor **1b** (right side of Figure 4). The destabilization of about 10 kcal mol^{-1} with respect to **2b** suggests that the first effect of the oxidation is the bending of the rider. On the other hand, the vibration mode of the imaginary frequency is indicative of the attempted rotation of the $Ru(CO)_3$ fragment (at the atom Ru2) about its 3-fold axis and toward the staggered geometry of **2b**. Notice that, while in our model all three CO ligands can interconvert, only an oscillation of the RuL_3 fragment is permitted in the actual system **2** due to the presence of the dppm ligand.

By monitoring the evolution of the frontier MOs in the system **b**, we gain a better understanding of the electron redistribution and the evolution of the chemical bonding upon oxidation. The HOMO and the LUMO of **2TS**, reported in Figure 5, are reminiscent of the two highest filled levels of **1a** (see Figure 3). Upon the bending of the rider, the M−M bonding character mixes with that of π_3*. In this manner, the two frontier MOs become mainly the bonding and antibonding counterparts for the back-donation of the Ru2 metal into the diimino rider. Since the M−M bonding character is shared by both the HOMO and the LUMO, the electron vacancy of the latter causes a significant Ru−Ru bond weakening (intermetallic separation at **2TS** = 2.928 Å, versus 2.583 Å for **1a**).

Due to the asymmetric shape of the d_π orbitals at the conical ML_3 fragments,[30] a 60° reorientation of the η^4-coordinated $Ru(CO)_3$ fragment increases significantly the d_π−π_3* interaction. This is evident by looking at the HOMO of **2b** (left side of Figure 6), while the LUMO, at the right side, is essentially the σ hybrid of the square pyramidal fragment at Ru1. In other words, the im-

(29) No dramatic changes were found in the calculations when the simpler DAD ligand was used in place of the *o*-phenylendiamido one. For instance, the model complexes $[Ru_2(\mu\text{-DAD})(\mu\text{-}H_2PCH_2PH_2)(PH_3)_2(CO)_2]$ and $[Ru_2(\mu\text{-DAD})(\mu\text{-}H_2PCH_2PH_2)(PH_3)_2(CO)_2]^{2+}$ show computed parameters close to those of **1a** and **2a**, respectively (see Supporting Information).

(30) (a) Elian, M.; Chen, M. M.-L.; Mingos D. M. P.; Hoffmann, R. *Inorg. Chem.* **1976**, *15*, 1148. (b) Albright, T. A.; Burdett, J. K.; Whangbo, M.-H. *Orbital Interactions in Chemistry*; Wiley: New York, 1985.

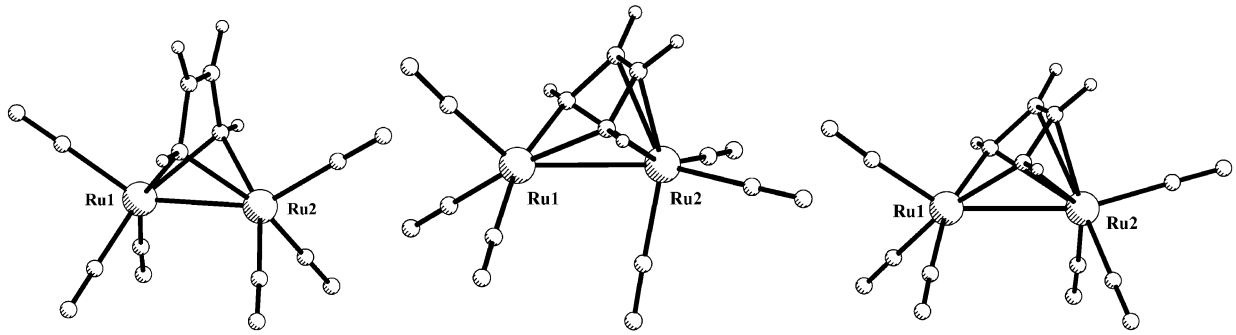

Figure 4. Optimized structures of $[Ru_2(DAD)(CO)_6]$ (**1b**), $[Ru_2(DAD)(CO)_6]^{2+}$ (**2b**), and $[Ru_2(DAD)(CO)_6]^{2+}$ (**2TS**).

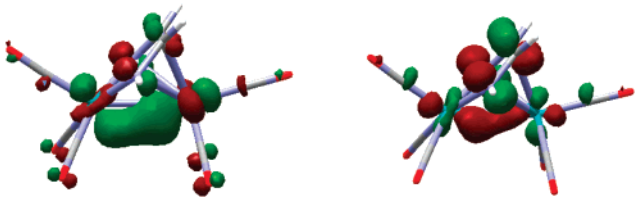

Figure 5. 3D isosurfaces corresponding to the HOMO and LUMO of **2TS**.

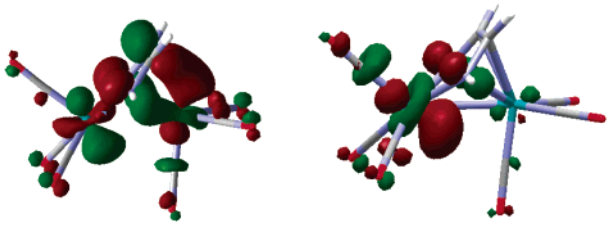

Figure 6. 3D isosurfaces corresponding to the HOMO and LUMO of **2b**.

proved back-donation from one metal determines an evident unsaturation of the other metal. Importantly, the HOMO−LUMO gap increases by 12.2 kcal/mol^{-1} on going from **2TS** to the stationary point **2b**.

As discussed above, the dications of type **2** can be described as formed by a diimino ligand bent over the d^7-d^7 Ru_2L_6 sawhorse. An equivalent metal oxidation states is suggested also by the similar charges of the two metals, although the Ru−Ru bond should be somewhat polarized. In fact, larger electrophilicity of the atom Ru1 is suggested by the LUMO of **2b** (Figure 6) and the atom Ru2 appears less negative than expected due to the back-donation toward the diimino ligand. In an extreme situation, there could be a metal−ligand charge transfer that restores the diamido character of the ligand (10-electron donor) and determines the oxidation of the metal atoms (d^6-d^6 configuration). Still a direct but weak M−M bond could be assumed due to the donation from a lower filled t_{2g} orbital of Ru2 into the empty σ hybrid of Ru1. Such a dative character of the M−M bond is also applicable to the d^7-d^7 description, as the HOMO of **2b** (Figure 6) maintains only a negligible Ru−Ru bent bond character.

Complex **1** was investigated electrochemically. The room-temperature cyclic voltammogram (CV) showed a quasi-reversible oxidation peak centered at $E_p = -0.02$ V (vs $Fe(Cp)_2$; $\Delta E_p = 0.42$ V). The coulometric measurements are consistent with a $2e^-$ process. Previously, we have highlighted the structural rearrangements produced in the oxidation of the system **1** to **2**. In particular between the models **1b** and **2b**, we detected **2TS** as a possible transition state in the overall oxidation process. Consequently, the equation in Scheme 4 may be proposed.

Scheme 4

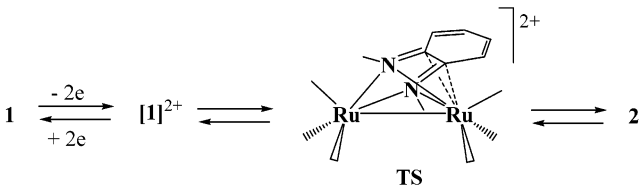

The removal of two electrons from **1** gives primarily the transient species $[\mathbf{1}]^{2+}$, which is likely unstable. The structural rearrangement to the final product **2** occurs through a transition state **TS**, which should be similar to **2TS**. The barrier associated with the **2** → **TS** reorganization (12.2 kcal/mol^{-1} computed for the system **b**) accounts for the electrochemical quasi-reversibility of the process.[31]

The oxidation reaction with $[Fe(Cp)_2]PF_6$ was carried out also for another analogue of **1** such as $[Ru_2\{\mu\text{-}C_6H_4(NH)_2\text{-}o\}(CO)_4(PPh_3)_2]$ (**3**). In this case, a crude dicationic product **4** was obtained with variations of the IR properties that are similar to those of **2** with respect to **1**. Thus the ν(NH) bands and the four ν(CO) bands are shifted to lower and higher frequencies, respectively. The $^{31}P\{^1H\}$ NMR spectrum may be interpreted in terms of two species that slowly evolve into two new ones (see the Experimental Section). All methods that tried to isolate a single compound were unsuccessful. To understand better the nature of the species, we optimized for $[Ru_2(DAD)(CO)_4(PH_3)_2]^{2+}$ five different isomers that differ in the relative orientation of the two terminal $Ru(CO)_2(PH_3)$ fragments. The Supporting Information presents pictures of all the stationary points **4a** through **4e** that are all close in energy (the maximum ΔE is 4.9 kcal mol^{-1}). Since the barrier for the rotation of the ML_3 fragment at the Ru2 atom was estimated to be about 10 kcal mol^{-1} for the system **2** (and it is probably higher in the presence of the actual PPh_3 ligand), the interconversion between the pairs of isomers **4a**−**4e** may be somewhat hindered. This can qualitatively explain the complicated $^{31}P\{^1H\}$ NMR spectrum as a result of the presence and the evolution of the different isomers.

Finally, the oxidation of the compound $[Ru_2\{\mu\text{-}C_6H_4(NH)_2\text{-}o\}(CO)_3(PPh_3)(dppe)]$ with $[Fe(Cp)_2]PF_6$ afforded a product of proposed formulation $[Ru_2\{\mu\text{-}C_6H_4(NH)_2\text{-}o\}$-

(31) Zanello, P. *Inorganic Electrochemistry. Theory, Practice, and Application*; Royal Society of Chemistry: Cambridge, UK, 2003.

$(CO)_3(PPh_3)(dppe)](PF_6)_2$ on the basis of IR and $^{31}P\{^1H\}$ NMR spectra. Crystals for X-ray diffraction analysis could not be obtained, and a structure of type **2** was again assumed for the dication. However, the Na/Hg reduction of this compound gave a mixture of complexes where only minor amounts of the precursor $[Ru_2\{\mu\text{-}C_6H_4(NH)_2\text{-}o\}(CO)_3(PPh_3)(dppe)]$ were detected. Further experimental and theoretical analyses would be necessary to understand better the nature of the system, but these have not been carried out as yet.

$MoRu_2$ Trinuclear Compounds. As mentioned, the synthesis and X-ray characterization of the complex $[Ru_2Mo\{\mu\text{-}C_6H_4(NH)_2\text{-}o\}_2(CO)_6(PPh_3)_2]$ (**5**) (see the structure in Scheme 2) have been previously presented.[12] Later, by using perturbation theory arguments (EHMO calculations),[15] we provided an explanation of why the highest possible C_{2v} symmetry is not attainable. As a matter of fact, the molecular symmetry is only C_2 with each terminal L_3Ru fragment (together with its associated and upright $C_6H_4(NH)_2$-*o* bridge) being rotated by about 30° with respect to the other. The lowering of the symmetry rearranges the coordination geometry about the Mo atom halfway between trigonal prismatic and octahedral. This permits the formation of two noncollinear Mo→Ru dative bonds thanks to the donations from two distinct t_{2g}-like Mo orbitals into the empty σ hybrids of the terminal L_5Ru fragments.

The oxidation of **5** with $[Fe(Cp)_2]PF_6$ (molar ratio 1:2), in CH_2Cl_2 solution, yielded the compound $[Ru_2Mo\{\mu\text{-}C_6H_4(NH)_2\text{-}o\}_2(CO)_6(PPh_3)_2](PF_6)_2\cdot CH_2Cl_2$ (**6**), which was isolated as a brown solid in high yield after the appropriate workup. No other reaction product was obtained after longer reaction times with an excess of oxidant. The reduction of **6** with sodium amalgam again afforded **5** in quantitative yields. The IR spectrum of **6**, besides the characteristic bands of the PF_6^- counterion, shows two ν(NH) weak bands at 3343 and 3303 cm^{-1}. This suggests that the ligand $C_6H_4(NH)_2$-*o* may be present in both the dianionic and neutral formulations. Additionally, the ν(CO) region displays a pattern of bands around 2000 cm^{-1}; that is, the bands are all shifted to higher values with respect to those of the parent complex **5**. In this respect, the bands of the Mo-coordinated carbonyl ligands seem to be more affected than those of the Ru-coordinated ones. The ^1H NMR spectrum shows a complex multiplet pattern for the phenyl ring protons and a broad signal for the four NH protons. Also, the ^{31}P NMR shows a singlet for the two PPh_3 ligands. Thus, it is not possible to distinguish between the arrangement of the two $C_6H_4(NH)_2$-*o* bridges most probably on account of a fluxional process that averages, on the NMR scale, the arrangement of the ligands.

The molecular structure of the complex dication in **6** is presented in Figure 7. Selected bond distances and angles are collected in Table 4, together with the calculated ones (vide infra).

There are some evident differences between the skeletons of the two redox derivatives **5** and **6**. For instance, the arrangement of the three metal atoms is definitely more bent in the oxidized complex (the angle Ru−Mo−Ru decreases from 167.1(2)° to 145.8(1)°). Also the quasi-C_2 symmetry of the precursor transforms into pseudo-C_s symmetry, the mirror plane passing through

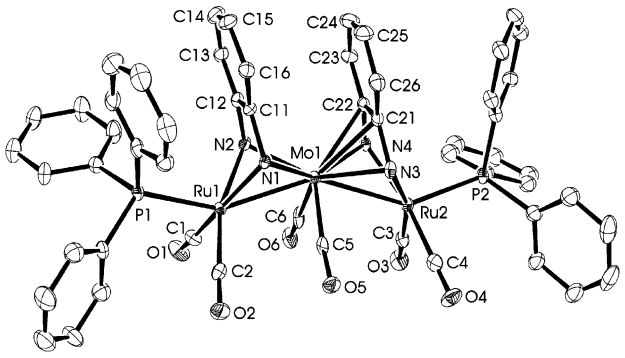

Figure 7. Molecular structure of the cationic part of complex **6**.

Table 4. Selected Structural Parameters of 6 and Calculated Model Compound 6a

bond distances (Å) and angles (deg)	complex **6** (exptl)	complex **6a** (calcd)
Ru1−Mo1	2.699(2)	2.789
Ru2−Mo1	2.792(2)	2.904
Ru1−N1	2.135(6)	2.156
Ru1−N2	2.133(6)	2.156
Ru2−N3	2.072(6)	2.108
Ru2−N4	2.099(6)	2.108
Mo1−N1	2.178(5)	2.231
Mo1−N2	2.195(6)	2.231
Mo1−N3	2.205(6)	2.294
Mo1−N4	2.198(6)	2.294
Mo1−C21	2.428(7)	2.449
Mo1−C22	2.439(7)	2.450
N1−C11	1.440(9)	1.445
N2−C12	1.439(9)	1.445
N3−C21	1.39(1)	1.381
N4−C22	1.402(9)	1.381
C11−C12	1.39(1)	1.337
C21−C22	1.42(1)	1.393
C22−C23	1.39(1)	
C23−C24	1.37(1)	
C24−C25	1.42(1)	
C25−C26	1.35(1)	
C26−C21	1.41(1)	
C12−C13	1.37(1)	
C13−C14	1.39(1)	
C14−C15	1.38(1)	
C15−C16	1.39(1)	
C16−C11	1.37(1)	
Ru1−Mo1−Ru2	145.8(1)	152.5
C5−Mo1−C6	84.5(4)	82.3
C1−Ru1−C2	92.7(4)	89.7
C3−Ru2−C4	88.8(4)	89.8
Ru1−N1−Mo1	77.5(2)	78.9
Ru1−N2−Mo1	77.1(2)	78.9
Ru2−N3−Mo1	81.4(2)	82.4
Ru2−N4−Mo1	81.0(2)	82.4

the metals and terminal phosphorus atoms. Thus the inner molecular torsion, highlighted for the precursor **5**, is now absent. In **6**, the terminal RuL_3 fragments eclipse each other and the central molybdenum atom approaches a much more regular trigonal prismatic coordination. On the other hand, the two $C_6H_4(NH)_2$-*o* ligands adopt two different bridging modes, i.e., upright and bent. Thus, the bridge over the Ru1−Mo bond is symmetrical, with the two equivalent Ru−N distances that are about 0.05 Å shorter than the Mo−N ones on account of the different metal radii (Ru(μ-N,N′)Mo bonding mode). In contrast, the ligand across the Mo and Ru2 atoms leans toward the former metal which is η^4-coordinated with the two Mo−C distances being as short as 2.428(7) and 2.439(7) Å. While the associated

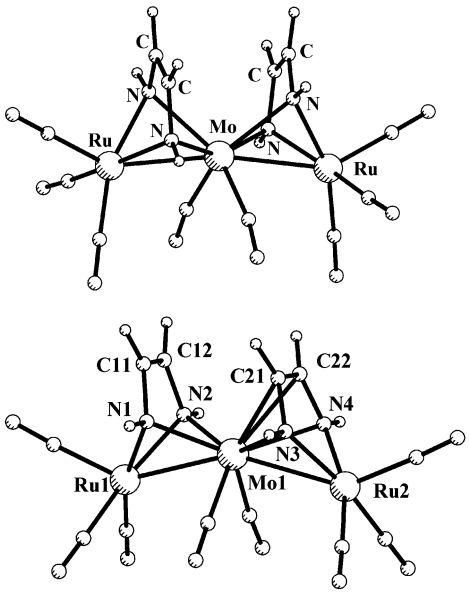

Figure 8. Optimized structures of $[Ru_2Mo(\mu\text{-DAD})_2(CO)_8]$ (**5a**) and $[Ru_2Mo(\mu\text{-DAD})_2(CO)_8]^{2+}$ (**6a**) model compounds.

Mo−N distances are essentially equal to those involving the upright bridge (about 2.20 Å), the Ru−N ones are correspondingly shorter (compare the average values of 2.080(7) and 2.134(6) Å). It is also interesting to compare the geometries of the different chelates. While in the upright one the C−C and C−N separations of 1.39(1) and 1.44(1) Å (av) are quite similar to those found in the precursor **5** (diamido character), the bent ligand shows elongation and shortening of the same bonds (1.420(10) Å for C−C and 1.395(10) Å (av) for C−N). In this case, the experimental structural data are of sufficiently good quality to assess prevailing C═N double and C−C single bonds within the bent ligand (*o*-diiminobenzene character).

As for the binuclear compounds, a DFT analysis was carried out for models of **5** and **6** in order to understand their electronic underpinnings. The computational burden was reduced by adopting the models $[Ru_2Mo(\mu\text{-DAD})_2(CO)_8]$ (**5a**) and $[Ru_2Mo(\mu\text{-DAD})_2(CO)_8]^{2+}$ (**6a**). The structures, optimized without symmetry constraints, are displayed in Figure 8, with the structural parameters for **6a** being reported in Table 4. Those of **5a** appear in Table 5 together with the experimental data for **5**. Despite the oversimplified models, the agreement with the experimental structures is acceptable. For instance, the distortion of the precursor from the highest possible C_{2v} symmetry is well reproduced as well as other minor details such as the ∼12° bending from linearity of the two Mo−C−O angles. On the other hand, the model **6a** has almost C_s symmetry with two nonequivalent chelate bridges. The computed Mo−Ru distances present the highest discrepancy (0.1 Å) with respect to the experimental data, a result that is not rare for model compounds where heavy metal atoms are weakly bonded.

As mentioned, we previously exploited qualitative MO arguments to highlight the dative nature of the Mo→Ru bonds in **5**.[15] The point is also supported by the present DFT calculations. For instance, the HOMO-3 and HOMO-4 (bottom of Figure 9) are quite similar to those of the EHMO method and are indicative of the donations from two distinct filled Mo d orbitals into the empty σ hybrids of the two Ru atoms. Moreover, the HOMO and HOMO-1, presented in the upper part of Figure 9, are quite close in energy and share the π_3* character of the bridging ligands (refer to Scheme 4) with some minor metal contribution. In this respect, the situation resembles that of the binuclear species **1a** and **1b**, where the HOMO has prevailing π_3* character.

Table 5. Selected Structural Parameters of Calculated Model Complex 5a and Comparison with X-ray Data

bond distances (Å) and angles (deg)	complex **5** (exptl)	complex **5a** (calcd)
Ru−Mo	2.700(2)	2.747
	2.708(2)	2.747
		2.138
Ru−N	2.12(1)	2.138
	2.15(1)	2.163
		2.163
Mo−N	2.19(1)	2.232
	2.26(1)	2.345
	2.20(1)	2.232
	2.24(1)	2.345
		1.424
N−C	1.41(1)	1.439
	1.42(1)	1.424
		1.439
C−C	1.39(1)	1.342
	1.40(1)	1.342
Ru−Mo−Ru	167.1(2)	168.7
OC−Mo−CO	81.5(5)	85.8

Analogously to the binuclear systems, the removal of one electron pair from the species of type **5** determines initially a small HOMO−LUMO gap that triggers, in turn, a Jahn−Teller effect. Ultimately, the two bridges acquire different diimino and diamido roles as it is inferred from their computed geometries in **6a**. The 1.381 Å N−C distances in the bent chelate are significantly shorter than those in the upright chelate (1.445 Å). At the same time, the C−C length is definitely longer in the bent ligand (1.393 vs 1.337 Å). We suggest the following qualitative MO arguments to interpret the evolution of the chemical bonding from **5** to **6**. In the latter, the five d orbitals of molybdenum are split according to the trigonal prismatic coordination. Thus, *xz* and *yz* are most destabilized and empty, z^2 is the lowest and nonbonding filled orbital, and finally the intermediate *xy* and x^2-y^2 orbitals are best suited to exert donor properties. As shown in Scheme 5 (right side), *xy* donates electrons into an *out-of-phase* combination of Ru σ hybrids (see the analogy with the HOMO-3 of the precursor **5**).

Conversely, x^2-y^2 (left side of Scheme 5) loses the original M_3 overall bonding character and becomes mainly involved in back-donation on bending one of the chelates (diimino acceptor). Since the LUMO of **6a** (see Figure 10) is mainly antibonding for the latter interaction, the gap with respect to the HOMO increases correspondingly. The LUMO also features some antibonding character for the subtended Ru−Mo vector, thus suggesting that the bond is not totally vanished. This is confirmed by its relatively small elongation of about 0.1 Å. In contrast, the effect of the oxidation on the M−M bond was dramatically larger (about 0.3 Å) for the dimeric redox systems of type **1** and **2**. Probably, this difference reflects the intrinsic weakness of the dative Mo→Ru bonds also in the precursor **5**.

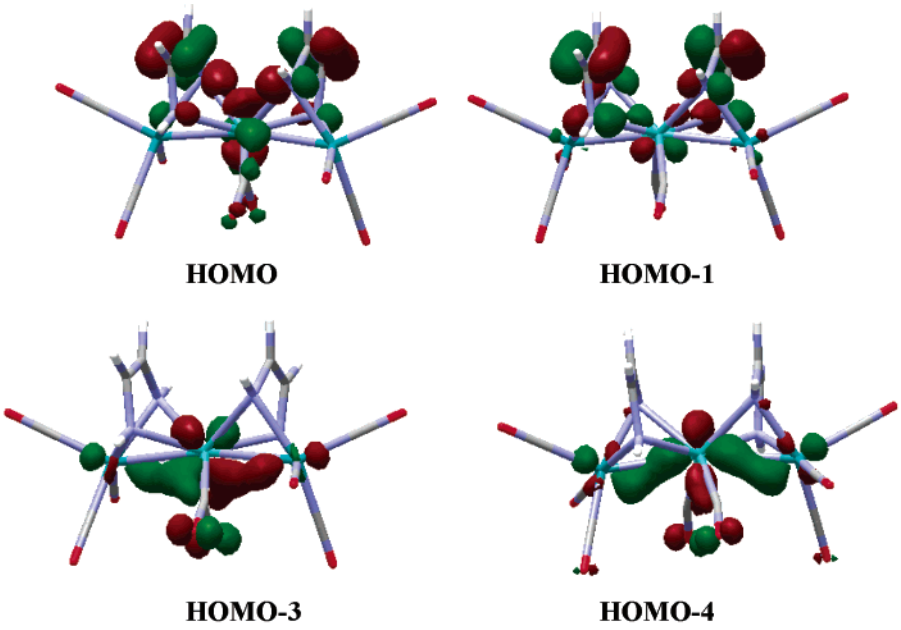

Figure 9. Some of the highest occupied molecular orbitals of **5a**.

Scheme 5

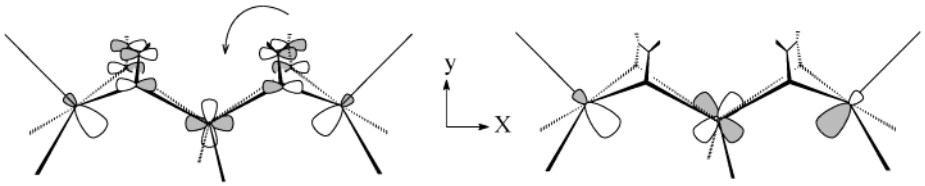

The electrochemistry behavior of complex **5** is similar to that of **2**. The CV shows a quasi-reversible two-electron oxidation process centered at about 0.30 V. (vs $Fe(Cp)_2$; $\Delta E_p = 0.14$ V). The interpretation of the CV is also parallel to that previously stated for binuclear **2**. The removal of two electrons on **5** gives species $[\mathbf{5}]^{2+}$, which are unstable due to a small HOMO−LUMO gap. Species $[\mathbf{5}]^{2+}$ rapidly converts into complex **6**.

Finally, we addressed theoretically the nature of the fluxional process that makes the two bridging chelates equivalent in the NMR scale. To this purpose, we have imposed in the dication $[Ru_2Mo(\mu\text{-DAD})_2(CO)_8]^{2+}$ a mirror plane passing through the Mo atom and its coordinated CO ligands. The optimized structure, reported in Figure 11, corresponds to an actual transition state, **6TS**. At the latter, the two chelates do not bisect their subtended Mo−Ru bonds because they are bent by about 16° both toward the central Mo atom. The vibration mode of the imaginary frequency shows *in-phase* oscillation of the two bridges. This allows one chelate to become almost perpendicular to the Mo−Ru bond (87° in **6a**), while the other adapts to the η^4-coordination at the molybdenum center (the corresponding angle is 60°). The calculated barrier for such a rearrangement is rather low (3.4 kcal mol^{-1}) and is fully in agreement with the NMR spectra that suggest a fast exchange regime at room temperature. Thus the different electronic structure highlighted for the two chelates in the oxidized trimer is subject to a fast equilibrium through the concerted movement of the two DAD ligands.

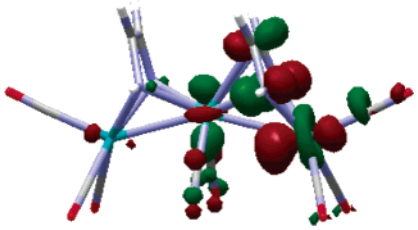

Figure 10. LUMO of **6a**.

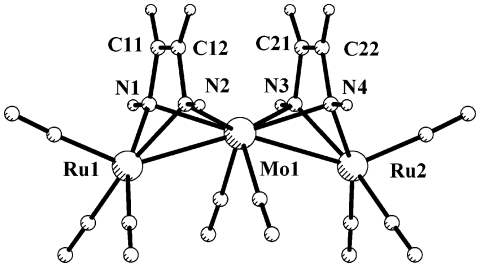

Figure 11. Optimized structure of $[Ru_2Mo(\mu\text{-DAD})_2(CO)_8]^{2+}$ (**6TS**) model compound.

Conclusions

The present paper has reported the interesting redox properties of binuclear and trinuclear systems where the M−M bond(s) is (are) bridged by *o*-phenylenediamido ligand(s). There is no doubt that the dianionic character is attributable to the bridging chelate(s) in all the precursor compounds. The primary effect of the oxidation is in general the transformation of the diamido into diimino character. Most interesting is the selective oxidation of only one of the two ligands in the trinuclear

$MoRu_2$ systems, which leads to the first structurally characterized complex that contains two adjacent *o*-phenylenediamido and *o*-diiminobenzene bridges. The latter are simultaneously bound to the central molybdenum atom with different coordination modes. The different character of the bridges is fully confirmed by the calculation of the gas-phase molecular model. Conversely, the NMR data in solution suggest equivalence or fast equilibrium between the two bridges. This result is fully consistent with the nature and low energetics of the transition state structure **6TS**. Through the combined experimental and theoretical studies, the structural and the electronic consequences of the oxidation of polynuclear *o*-phenylenediamido complexes have been properly highlighted for what concerns, in particular, the evolution of the chemical bonding.

Acknowledgment. Financial support from CICYT (BQU2000-0219, BQU2001-3715, and BQU2000-0227), the Principado de Asturias (PR-01-GE-6 and PR-01-GE-04), and the Secretaría de Estado de Educación y Universidades (sabbatical stay at ICCOM, A. G.) are gratefully acknowledged. The quantum-chemical calculations were carried out by exploiting the High Performance Systems of the Centro di Calcolo Interuniversitario CINECA (CNR-CINECA agreement).

Supporting Information Available: CVs for complexes (Figures S1 and S2). Selected computed parameters and optimized structures of several model compounds (Tables S1−S5). CIF files for **2** and **6**. This material is available free of charge via the Internet at http://pubs.acs.org.

OM034223K